Analysis of the Flow Conditions in the Ova Spin Pumped Storage Plant and their Impact on Acoustic Discharge Measurement

F. Fahrni[1], T. Staubli[1,2], U. Gerold[2]

[1]*Hochschule Luzern, Technik &Architektur, 6048 Horw, Switzerland*
[2]*etaeval GmbH, 6048 Horw, Switzerland*

thomas.staubli@etaeval.ch

Abstract

For the circular measuring cross sections of the Ova Spin pumped storage plant numerical flow simulations (CFD) were performed in the context of the installation of the acoustic transit time flow meter. These simulations were needed because the position of the installation of the flow meter is far from being ideal. In pump direction a bend followed by a convergent section cause strong Dean vortices and in turbine direction the measuring section is immediately downstream of two butterfly valves. The flow rate data evaluated with Gauss Jacobi weights had to be corrected differently in pump and turbine directions. These corrections were independent on the flow rate itself. Measurements of the path velocities at different operating points confirmed the independence of the velocity distributions from the flow rate, and they also agreed well with the simulated path velocities, verifying the correctness of the simulated distributions. In turbine direction the flow meter does not detect the velocity deficit in the center due to the wake of the valves and therefore significantly overestimates the flow rate. In pump direction the Dean vortices entrain flow with low velocities in the middle of the flow cross section which is also not detected by the flow meter and the flow rate is also overestimated to some extend. The overall measuring uncertainty is determined as ±0.77 % in turbine direction and as ±0.66 % in pump direction.

1. Introduction

The Ova Spin power plant of the Engadiner Kraftwerke is a pumped storage power plant with a capacity of 50 MW and is located on the Inn river basin in Switzerland. It processes the water from Lago di Livigno and discharges it into the equalizing basin of Lai da Ova Spin. During off-peak periods, the water is pumped from the equalization basin back into Lago di Livigno. The powerhouse is located in a cavern below the overflow dam wall of the Lai da Ova Spin. Two vertical axis reversible pump-turbines are installed.

As no suitable location for the installation of an acoustic transit time meter (ATT) could be found in the powerhouse, it was decided to install it at the only accessible location in the valve chamber below the Punt dal Gall arch dam on lake Livigno. However, the flow conditions at this point are anything but ideal. In the pumping direction, the flow is distorted by a bend and an asymmetrical contraction, and in the turbine direction the measuring section is located in the wake of two butterfly valves connected in series, Fig. 1 and 2.

The flow meter consists of 8 acoustic paths on two crossed planes. The layer positions of the sensors are selected according to Gauss-Jacobi, as described in IEC 60041. For reasons of space, the angle of the planes was set at 65 degrees. The layers were tilted at an angle of 10 degrees, Fig. 3. In the case of turbine operation, this leads to the positive effect that at least paths 3 and 8 are slightly affected by the wake of the valves and thus the velocity distribution is averaged to a certain degree.

The results of the flow simulations (CFD) are presented below and the simulated path velocities are compared with the measured ones. Since the velocity distributions are far from ideal ones, correction factors are introduced, which take into account the differences between the flow rate evaluated with the Gauss Jacobi weights and the flow rate given in the CFD simulation. The option of using different weights for the path velocities based on the simulations in pump mode operation and turbine mode operation was unfortunately not feasible. The correction factors, on the other hand, were easily implemented in the system. The correction in pump direction was -0.53 % and in turbine direction -1.05 %.

After installation, geometrical measurements were carried out using a theodolite. The average pipe diameter was determined to be D = 2.593 [m] and the exact path lengths, angles and positions of the sensor pills were also measured.

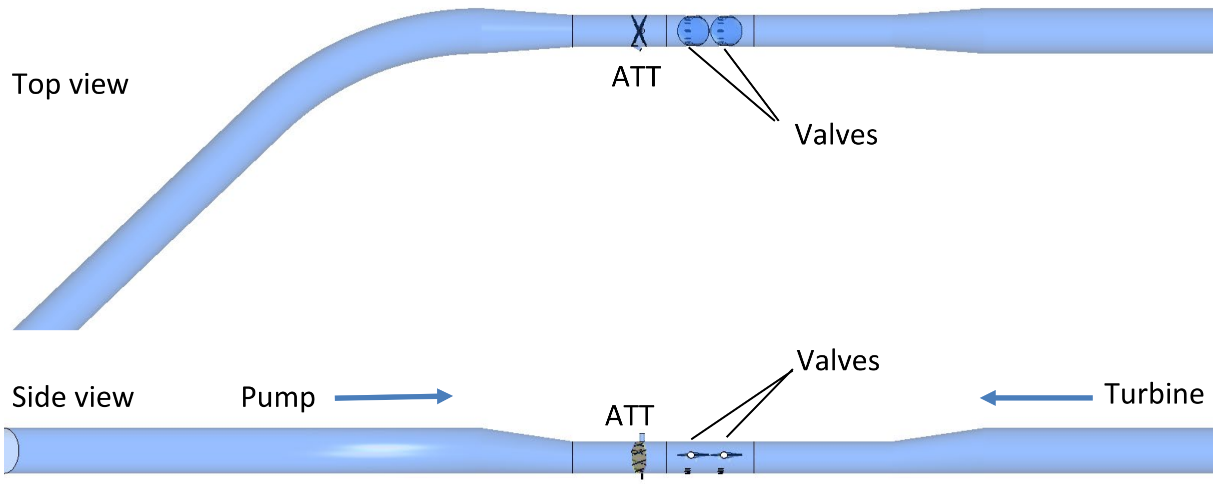

Figure 1 Layout of the ATT flow meters in the valve chamber

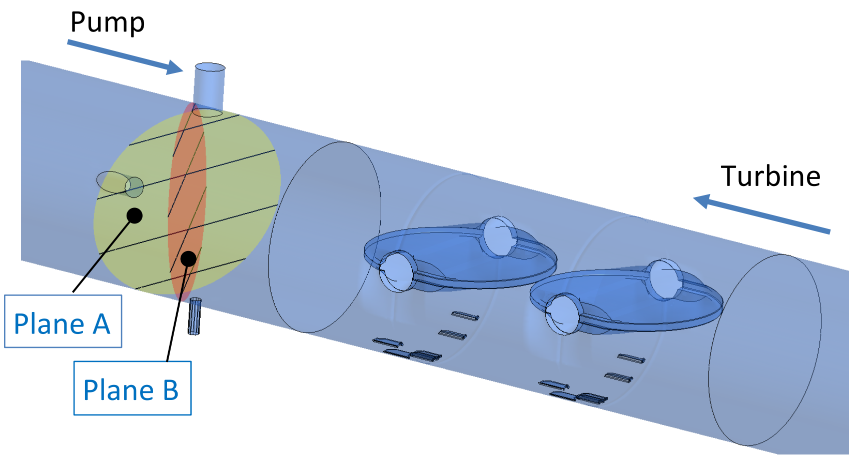

Figure 2 Location of the flow meter in the vicinity of the butterfly valves

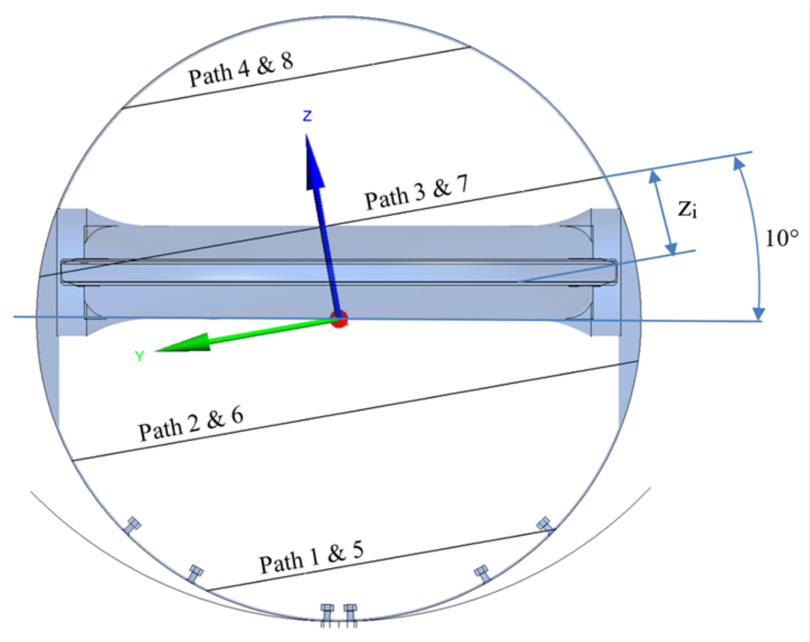

Figure 3 Alignment of the acoustic paths in the measuring section.

Based on the knowledge of the distorted flow fields, it was decided to perform in-depth computational fluid dynamics (CFD) simulations and a detailed analysis of the measurement uncertainty [1]. Previous experience with such simulations is e.g. described in [2].

2. Numerical studies

Ansys CFX 19.2 was used to simulate the flow field assuming a three-dimensional incompressible steady-state flow field. The program solves the conservation equations for mass, momentum and energy. The discretization is performed by the finite volume method. The solutions are based on the SST (shear stress transport) turbulence model. The calculations are solved with the high-resolution advection scheme and with a physical timescale of 3 seconds.
Four operating points at different flow rates in turbine direction and four operating points in pump direction were simulated, as listed in Table 2.

2.1 Grid generation

The computational grid was generated with the program Pointwise 2022. The mesh of the conduit was a manually generated structured hexahedral mesh except for the butterfly valves, which were meshed in an unstructured manner. The mesh was built in such a way, that no interfaces between the domains were needed. Like this, the transition between structured and unstructured mesh is 1:1. To achieve higher resolution in the boundary layer, the mesh on the wall was refined along the entire penstock.
Important factors for a good convergence and accuracy of the results are the number of elements, the minimum and the maximum angles of the elements, the volume ratio between neighboring elements and the targeted dimensionless wall distance y^+.

Table 1: Meshing statistics

Total number of elements	$11.132 \cdot 10^6$
Hexahedral elements	$7.946 \cdot 10^6$
Tetrahedral elements	$2.495 \cdot 10^6$
Pyramids	$0.330 \cdot 10^6$
Prisms	$0.361 \cdot 10^6$
Maximum angles	<150° in 99.4% of elements (mean 102.1°)
Minimum angles	>25° in 97.9% of elements (mean 68.4°)
Volume ratio	< 5 in 96.4% of elements (mean 1.7)
y+	40…150

2.2 Boundary conditions

In a first step, fully developed velocity profiles for all flow rates were simulated with a short straight section with translational periodic boundary conditions. These velocity profiles with the given flow rates were then in a second step set as boundary condition at the inlet of the simulation domain.
The outlet boundary condition was set to a relative pressure of 0 Pa in each case. The walls are specified as ‘no slip walls’ assuming a wall roughness of 0.5 mm as they are aged concrete walls. The temperature of the water was set to 10 degrees.

2.3 Concept of the area flow function

The concept of the area flow function (AFF) was developed by Voser [3]. In his thesis he describes in detail the Gauss-Jacobi quadrature procedure. The AFF describes the distributions of the velocities averaged over the local conduit width as a function of the height (vertical coordinate z). Assuming an uniform velocity distribution, which is the assumption behind the Gauss Jacobi weights, in the circular flow cross-section, the AFF becomes a semicircle, as described in [4].

$$F(z) = \bar{v}_{ax}(z) \cdot b(z) \left[\frac{m^2}{s}\right] \tag{1}$$

In CFD *F(z)* is not a continuous function but a series of *N* values, typically a few hundred values.

$$F_{CFD}(z_i) = \bar{v}_{ax}(z_i) \cdot b(z_i) \left[\frac{m^2}{s}\right] \tag{2}$$

The AFF of the simulated velocity distribution in pump direction, normalized as explained below, is displayed in Figure 6 and the one in turbine direction in Figure 8.
To compare the theoretical, simulated or measured AFFs for various operating points, it is advisable to convert the AFF into a dimensionless form by introducing:

$$F(\zeta_i) = \bar{v}_{ax}(\zeta_i) \cdot \beta_i \; [-] \tag{3}$$

where:

$$\zeta_i = \frac{z_i}{D/2}, \qquad \beta_i = \frac{b(z_i)}{D}, \qquad \bar{v}_{ax\,norm}(\zeta_i) \cdot \beta_i = \frac{\bar{v}_{ax}(z_i) \cdot I \cdot D \cdot b(z_i)}{Q \cdot 2} \tag{4}$$

D [m] is the diameter, *Q* [m³/s] the flow rate and *I* the integration constant.

Integration constants I for the Gauss Jacobi weighted integration or the optimized weighted integration (OWICS) are:

$$I_{GJ} = \int_{-1}^{1} (1-\zeta^2)^{0.5} d\zeta = \frac{\pi}{2} = 1.57080, \qquad I_{OWICS} = \int_{-1}^{1} (1-\zeta^2)^{0.6} d\zeta = 1.51336 \tag{5}$$

If CFD area flow functions are compared with measured values based on Gauss-Jacobi weighting, I_{GJ} must be used to normalize the CFD data, and if they are compared with OWICS-weighted data, I_{Owics} has to be taken.
In the Ova Spin power plant, the decision was made to use the Gauss-Jacobi weighting due to the rather uniform velocity distribution in the pumping direction.

The AFF of the Gauss Jacobi integration is a semicircle. In non-dimensional form it is described with Eq. 6.

$$F_{GJ\,norm}(\zeta) = (1-\zeta^2)^{0.5} \quad [-] \tag{6}$$

2.4 Flow rate determination
With Gauss-Jacobi, the flow rate is approximated by weighting the measured velocities in the four layers in which the paths are crossed:

$$Q_{GJ} = \frac{D}{2} \cdot \sum_{i=1}^{N=4} w_{i,GJ} \cdot b_i \cdot v_{ax_i} \tag{7}$$

The velocity $v_{ax,i}$ is the axial layer velocity determined from the two crossed path velocities. In the measurements the width b_i is averaged from the measured path length L_i projected on the same layer.

$$b_i = L_i \cdot \sin(\varphi) \tag{8}$$

With φ the angles of the paths, as defined in IEC 60041.

3. Flow visualization

In the pumping direction, the flow is strongly influenced by the upstream bend and the asymmetrical contraction at about 2D before entering the measuring section. The bend leads to a pronounced formation of the counterrotating Dean vortices and the convergence to a more uniform distribution, which explains why the measured and simulated points lie well on the theoretical Gauss Jacobi AFF. On the other hand, we observe a large area with reduced velocities in the center, which is induced by the secondary flow, Figure 4 left. This velocity deficit cannot be detected by the acoustic paths, also indicated in Figure 4. Accordingly, one has to expect that the integration using Gauss Jacobi weights will result in too high flow rates. An upstream effect of the valves is not discernible.
In the turbine direction the velocity distributions are heavily distorted by the two butterfly valves immediately upstream. Four secondary vortices with low velocities in their core region can be observed. These vortices are formed by the lateral displacement flow of the two valves. In the center, a velocity deficit can be identified in a horizontal plane, which is due to the wake flow. Most of the vortex cores with low axial velocities are located in between acoustic paths and also the wake of the valves does not affect much the velocities on the paths. For this reason, an even higher overestimation of the flow rated based on the information of the path velocities in turbine direction occurs.

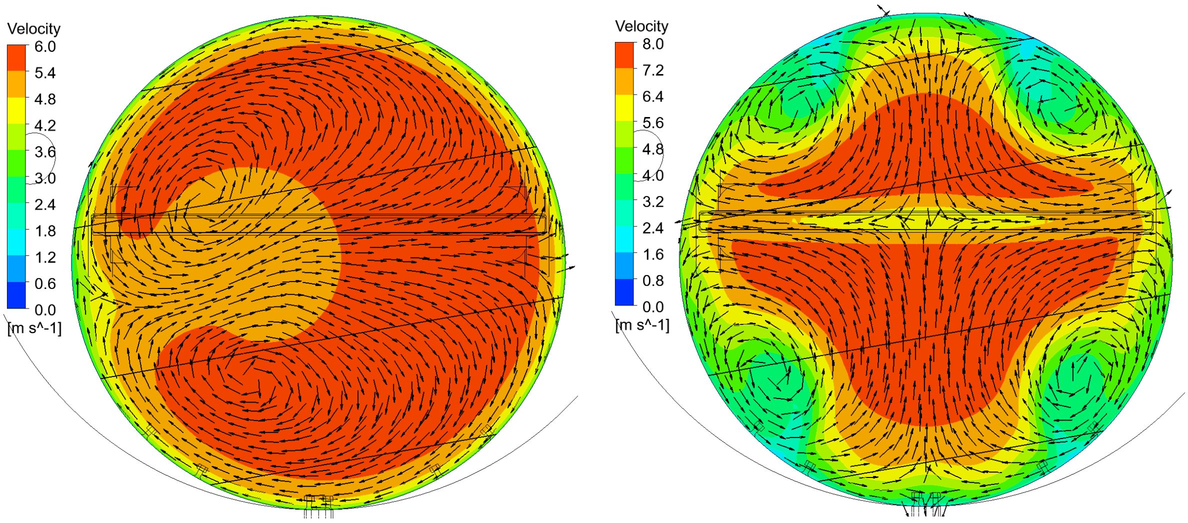

Figure 4 Velocity distributions in the measuring plane and projection of normalized transverse velocity vectors in pumping direction at 28 m^3/s (left) and in turbine direction at 32 m^3/s (right).

Figure 5 shows a side and top view of the turbine flow at 32 m^3/s with more details. The flow is from right to left. The blue areas indicate the dead water in the wake of the valves. The side view in particular shows that the wake is maintained for long distances. This wake hardly affects path 3&7 and all other paths are unaffected.

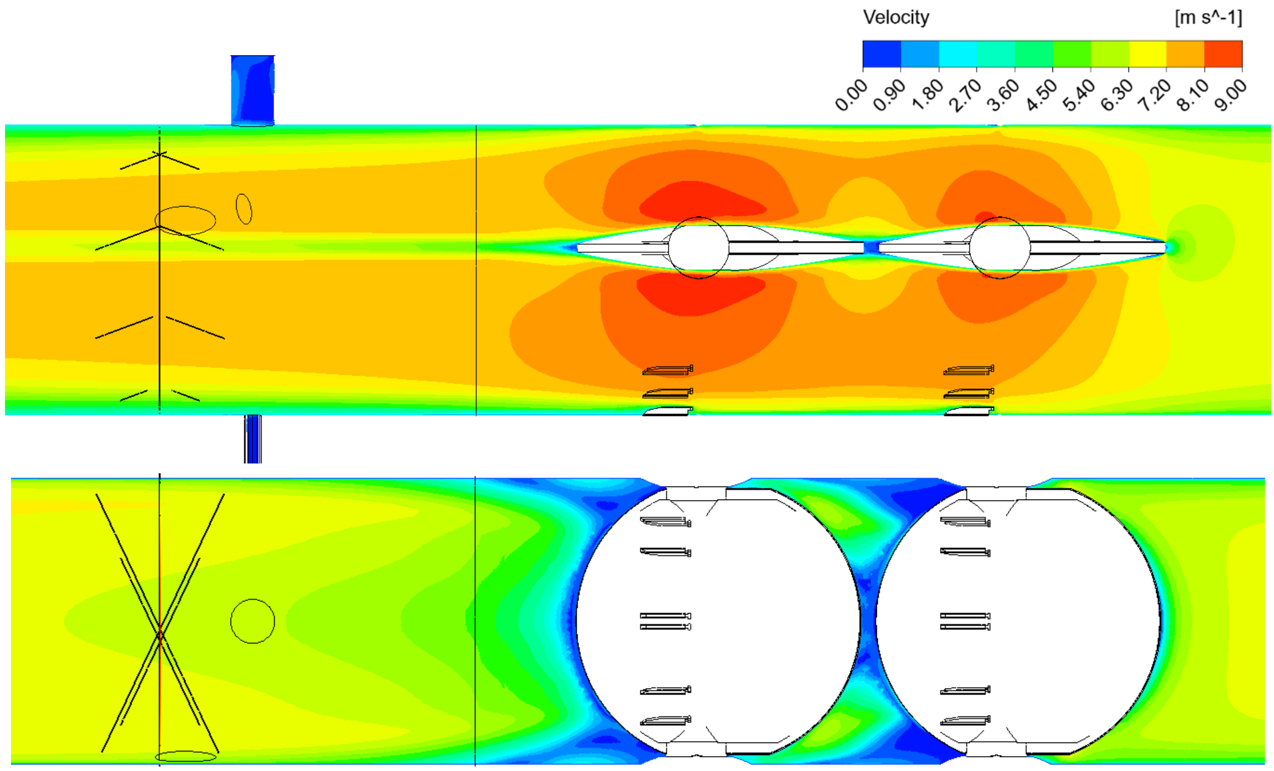

Figure 5 Side and top view of the velocity distributions in turbine direction at 32 m^3/s.

4. Investigated cases

Four operating points were simulated in both the pump and turbine directions at approximately one quarter, half, three quarters and maximum flow. The maximum flow rate in the turbine direction was 32 m^3/s and 28 m^3/s in the pump direction. Plotting all cases in non-dimensional form showed that there are no discernible differences in the distribution for the four simulated cases in pump direction and for the four cases in turbine directions. For this reason, only the CFD data of the maximum flow rates are presented in Figure 4 and 5 and in the following analysis of the area flow function and of the transverse flow.

Table 2: Simulated cases

Designation	Flow rate [m^3/s]	Operation
P_Q28	28.0417	Pump
P_Q20	20.0316	Pump
P_Q14	13.9734	Pump
P_Q7	6.9928	Pump
T_Q32	31.9756	Turbine
T_Q24	24.0165	Turbine
T_Q16	16.0109	Turbine
T_Q8	8.0126	Turbine

On the other hand, far more cases were measured on four different days. A series of measurements for pump operation is shown in Figure 6. The crosses of the different measuring points are hardly distinguishingly and do not depend on the flow rate. The red curve of the AFF of the simulation at 28 m^3/s and the blue curve of the Gauss Jacobi AFF are very close to each other. The faster decrease in the simulated AFF near the wall can be explained physically by the effect of the boundary layer. The measurements lie perfectly on the Gauss Jacobi distribution, which could lead to the erroneous conclusion that the Gauss Jacobi weighting is perfect for this case, but as mentioned above the local velocity deficits in between the Dean vortices are not reflected by the measurements. The measured and simulated transverse velocities, which are induced by the Dean vortices are depicted in Figure 7. Again, we observe here only a minor dependence of the strength of the transverse flow on the flow rate (transverse velocities are non-dimensioned with the corresponding axial velocity). Transverse velocities with a magnitude of 6 percent of the axial velocities are considered as high and without in depth numerical studies no installation of an acoustic flow meter should be considered. The numerically predicted transverse velocities seem to underpredict slightly the strength of the Dean vortices.

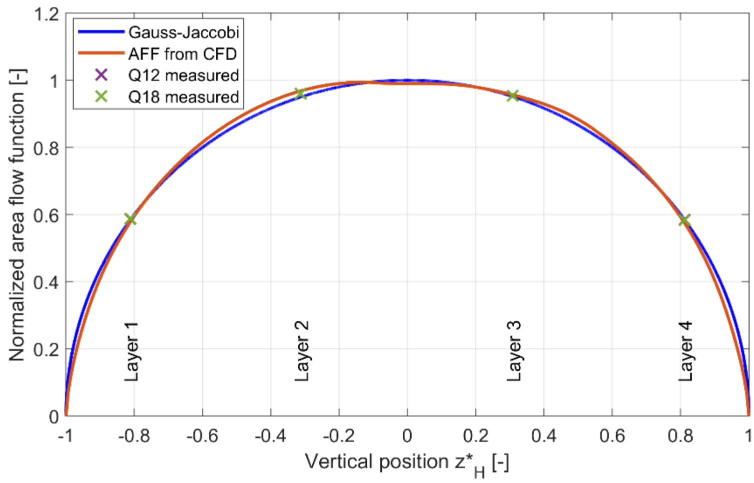

Figure 6 Comparison of AFFs in pump direction.

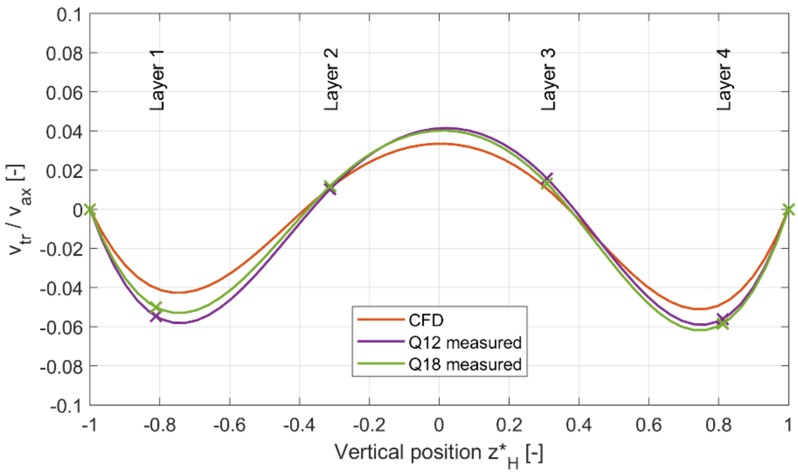

Figure 7 Transverse flow in pump direction

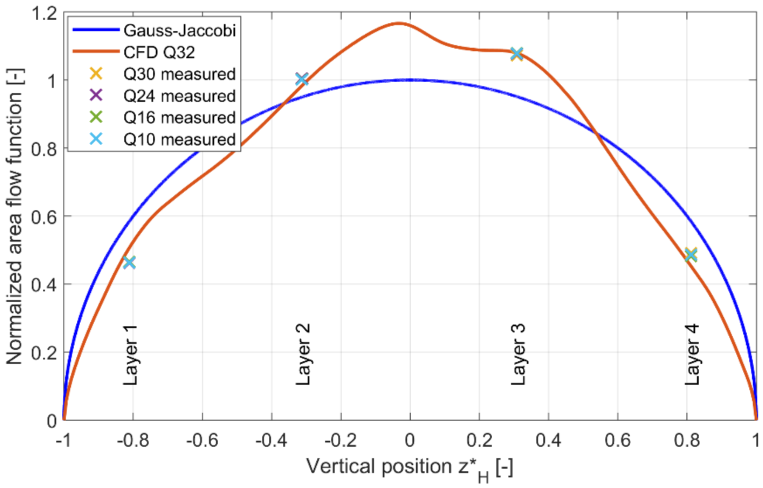

Figure 8 Comparison of AFFs in turbine direction.

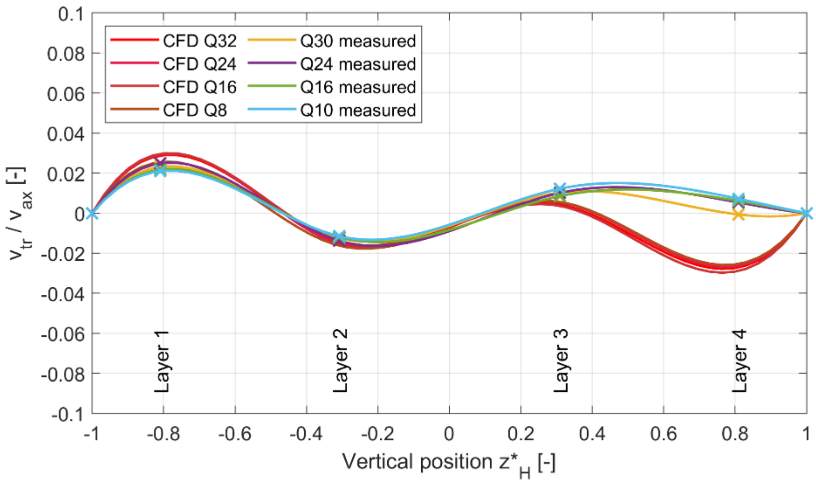

Figure 9 Transverse flow in turbine direction.

In the turbine flow direction, the simulated AFF deviates significantly from the Gaussian Jacobi distribution, Figure 8. The measured data points indicate that the simulation covers the main characteristics of this distorted flow field well. The transverse velocity component shown in Figure 9 is also well predicted for layers 1 to 3. However, the deviation is large for layer 4. The reason for this deviation could not be found. Maybe the vortical structures, as shown in Figure 4, right, are not well predicted in CFD.

The deviation of simulated or measured data on the individual paths from the reference AFF is an important quantity to judge whether the velocity distribution in the conduit is heavily distorted or if some of the path readings might be in error for any reason.

For this purpose, we define the following difference, as introduced in [4]:

$$\Delta F_i = \bar{v}_{ax\ norm\ GJ}(\zeta_i) \cdot \beta(\zeta_i) - F_{ref\ norm}(\zeta_i) \tag{9}$$

Depending on the differences to be considered we distinguish $\Delta F_{i\ \mathrm{CFD}-Meas}$, $\Delta F_{i\ GJ-Meas}$ or $\Delta F_{i\ GJ-CFD}$

An initial check should consist of determining the sum of this difference. This sum should be evaluated for control purposes. If this sum is not zero, the normalization procedure of the AFF may not have been carried out correctly.

$$\sum_{i=1}^{N} w_i \cdot \Delta F_i \ \approx 0 \tag{10}$$

On the one hand, the absolute maximum deviations are of interest, which make it possible to assess the agreement of measurements or CFD data with the underlying weighting function, Gauss-Jacobi or eventually OWICS, or the deviation between CFD simulations and measurements. This maximum deviation helps to identify weak points in the measurements and invites you to check all programming parameters for the layer with the maximum deviation.

$$\Delta F_{max} = \max|\Delta F_i| \tag{11}$$

Statistical quantities such as the weighted average absolute deviation or a weighted squared standard deviation are also indicators for the deviation from a reference AFF.

$$\mu = \frac{\sum_{i=1}^{N} w_i \cdot |\Delta F_i|}{\sum_{i=1}^{N} w_i} \tag{12}$$

$$\sigma = \sqrt{\frac{\sum_{i=1}^{N} w_i \cdot \Delta F_i^{\,2}}{\left(\sum_{i=1}^{N} w_i\right) - 1}} \tag{13}$$

The results of such an analysis of the deviations for the Ova Spin measurement are listed in Table 3. The numbers presented are averaged values from the various simulated and measured cases. The individual data between the operating points are scattered only insignificantly, therefore only the averaged deviations of all points are listed. Obviously, the maximum deviations and also the other statistical quantities are much larger for the highly distorted flow in turbine operation.

Table 3: Statistics of deviations

	ΔF_{max} CFD-Meas	ΔF_{max} GJ-Meas	ΔF_{max} GJ-CFD
Pump	0.0147	0.0036	0.0094
Turbine	0.0544	0.1284	0.1315
	μ |CFD-Meas|	μ |GJ-Meas|	μ |GJ-CFD|
Pump	0.0060	1.42E-05	0.0076
Turbine	0.0192	0.08910	0.0886
	σ CFD-Meas	σ GJ-Meas	σ GJ-CFD
Pump	6.47E-06	2.67E-05	3.32E-06
Turbine	1.50E-03	1.91E-02	1.16E-04

4. Uncertainty

To estimate the uncertainty of acoustic discharge measurement several uncertainties have to be taken into account. In a first step, the uncertainty, which arises by applying the equations which are needed to get the flow rate Q from the transit times and transit time differences, is analyzed. In a second step, the influence of the flow field on the accuracy is examined (integration error, protrusion error, ambient influence, unsteady flow conditions). The associated errors are systematic and/or random depending on the kind of error that is analyzed. The treatment of the errors follows in the basics the definitions and guidelines of the Standard IEC 60041:1991. Errors that follow a uniform distribution are marked with the letter *d*. Environmental influences are treated as purely random measurement uncertainties with a standard deviation σ_{amb}. The error of the flow rate f_{flow} is the result of a detailed analysis of the flow meter installation, including dimensions, lengths, angles and time measurements and is additionally also Students't value corrected.

For the presented Ova Spin measurement, the following values were determined for the errors mentioned above:

- Errors in the determination of the flow rate Q from the transit times:
  $f_{flow} = 0.56\ \%$
- Integration error:
  $d_{int} = 0.2\ \%$ in pump mode
  $d_{int} = 0.4\ \%$ in turbine mode
- Protrusion error:
  $d_{prot} = 0.1\ \%$
- Ambient influences:
  $\sigma_{amb} = 0.1\ \%$
- Unsteady flow conditions:
  $d_{unsteady} = 0.1\ \%$

The calculated overall uncertainty of the flow rate Q for a confidence interval of 95 % is:

$$f_{total,\sigma} = \pm 2\sqrt{\left(f_{flow,\sigma}/2\right)^2 + (\sigma_{int})^2 + \left(\sigma_{prot}\right)^2 + (\sigma_{amb})^2 + \left(\sigma_{unsteady}\right)^2} \tag{14}$$

$$f_{total,\sigma} = \pm 2\sqrt{\left(f_{flow,\sigma}/2\right)^2 + \left(\frac{d_{int}}{\sqrt{3}}\right)^2 + \left(\frac{d_{prot}}{\sqrt{3}}\right)^2 + (\sigma_{amb})^2 + \left(\frac{d_{unsteady}}{\sqrt{3}}\right)^2} \tag{15}$$

In pump mode:

$$f_{total,\sigma} = \pm 2\sqrt{\left(\frac{0.56}{2}\right)^2 + \frac{0.2^2}{3} + \frac{0.1^2}{3} + 0.1^2 + \frac{0.1^2}{3}} = \pm 0.66\ \% \tag{16}$$

In turbine mode:

$$f_{total,\sigma} = \pm 2\sqrt{\left(\frac{0.56}{2}\right)^2 + \frac{0.4^2}{3} + \frac{0.1^2}{3} + 0.1^2 + \frac{0.1^2}{3}} = \pm 0.77\ \% \tag{17}$$

5. Conclusion

In the knowledge that the velocity distributions in the measuring section of the flow meter installed at the Ova Spin hydropower plant will be highly distorted, detailed CFD studies were carried out. Since the velocity distributions in the pump and turbine directions differ significantly, and since a zone of velocity deficit not captured by the acoustic paths was found in the central part of the conduit in both flow directions, it was decided to introduce a flow correction for each pump and turbine operation instead of applying different OWISS weights (optimized weights for simulated sections).

In pump direction the flow field is dominated by the formation of Dean vortices due to an upstream bend. The convergent section further enhances the associated vorticity. The measured transverse velocities confirm well the existence of the secondary flow and indicate that the simulation slightly underpredicts the secondary flow. Since the velocity deficit due to the Dean vortices in the center of the conduit is not completely covered by the inner paths the correction amounted to -0.53 %.

In the turbine direction, the flow is distorted much more strongly by the two valves. In the simulation, two vortex-like flow structures are predicted above and two below the valves. The predicted and measured transverse velocities on the uppermost layer show inexplicable differences, while on the other layers the agreement is good. The wake behind the valves is only partially covered by the inner path, which leads to a considerable overestimation of the flow rate. The correction in turbine direction amounted to -1.05 %. This correction, however, is taken into account by assuming a larger integration uncertainty. The overall measuring uncertainty is determined as ±0.77 % in turbine direction and as ±0.66 % in pump direction.

Acknowledgements
The authors would like to thank the Rittmeyer company for providing the data as a basis for the simulations and analysis, as well the Engadiner Kraftwerke for permission to present the results of this study.

Terminology

d_{int}	%	integration error
d_{prot}	%	protrusion error
$d_{unsteady}$	%	error of unsteady flow conditions
f_{flow}	%	error in the determination of the flow rate Q from the transit times
$f_{total,\sigma}$	%	overall uncertainty of the flow rate Q for a confidence interval of 95 %
L_i	m	measured path length at elevation z_i
I_{GJ}	-	Integration constant for Gauss Jacobi weighted integration
I_{OWICS}	-	Integration constant for optimized weighted integration
φ_i	°	measured path angle at elevation z_i
v_{ax_i}	m/s	measured axial layer velocity at elevation z_i
$\bar{v}_{ax}(z)$	m/s	averaged measured axial layer velocity at elevation z_i
$\bar{v}_{ax}(z_i)$	m/s	averaged, simulated axial layer velocity at elevation z_i
$\bar{v}_{ax}(\zeta_i)$	-	normalized axial layer velocity at elevation ζ_i
$\bar{v}_{ax\ norm}(\zeta_i)$	-	normalized axial layer velocity at elevation ζ_i
$\bar{v}_{ax\ norm\ GJ}(\zeta_i)$	-	normalized axial layer velocity with Gauss Jacobi integration at elevation ζ_i

v_{tr_i}	m/s	measured transverse layer velocity at elevation z_i
Q	m^3/s	discharge, flow rate
Q_{GJ}	m^3/s	flow rate calculated with the Gauss Jacobi weighting
D	m	diameter
$w_{i,GJ}$	-	Gauss Jacobi weighting factor
b_i	m	width of conduit at elevation z_i
z	m	vertical coordinate
$z_H^* = 2 \cdot z/D$	-	nondimensional vertical coordinate
$F(z)$	m^2/s	area flow function AFF
$F_{CFD}(z)$	m^2/s	area flow function AFF of the simulated velocity distribution
$F(\zeta_i)$	-	nondimensional area flow function AFF
$F_{GJ\ norm}$	-	normalized area flow function AFF of the Gauss Jacobi integration
$F_{ref\ norm}$	-	normalized reference area flow function AFF
ΔF_i	-	deviation of simulated or measured data from the reference AFF
ΔF_{max}	-	absolute maximum deviation
β_i	-	nondimensional width of conduit at elevation
ζ_i	-	nondimensional vertical coordinate
μ	-	weighted average absolute deviation
σ	-	weighted squared deviation
σ_{amb}	-	uncertainty of ambient influences

References

[1] Gruber P., “Typical uncertainty analysis of acoustic discharge measurements by multipath flow meters in hydropower applications”, IGHEM2022, Grenoble, France, 2022
[2] Gruber P., Staubli T., Widmer M., Lüscher B., Widmer C., Roux L., “Multipath acoustic discharge measurement in non-standard situations”, HYDRO 2009, Lyon, France, 2009
[3] Voser A., “Analyse und Fehleroptimierung der mehrpfadigen akustischen Durchflussmessung in Wasserkraftanlagen”, ETH Zürich, Dissertation Nr. 13102, 1999
[4] Staubli T., Fahrni F., Gruber P., “Diagnosis of Acoustic Transit Time Data based on the Area Flow Function”, IGHEM2018, Beijing, China, 2018